TU Delft

Delft University of Technology

Quantitative MRI protocol and decision model for a 'one stop shop' early-stage Parkinsonism diagnosis

Study design

Seada, Samy Abo; van der Eerden, Anke W.; Boon, Agnita J.W.; Hernandez-Tamames, Juan A.

DOI
10.1016/j.nicl.2023.103506

Publication date
2023

Document Version
Final published version

Published in
NeuroImage: Clinical

Citation (APA)
Seada, S. A., van der Eerden, A. W., Boon, A. J. W., & Hernandez-Tamames, J. A. (2023). Quantitative MRI protocol and decision model for a 'one stop shop' early-stage Parkinsonism diagnosis: Study design. *NeuroImage: Clinical*, *39*, Article 103506. https://doi.org/10.1016/j.nicl.2023.103506

Important note
To cite this publication, please use the final published version (if applicable).
Please check the document version above.

Copyright
Other than for strictly personal use, it is not permitted to download, forward or distribute the text or part of it, without the consent of the author(s) and/or copyright holder(s), unless the work is under an open content license such as Creative Commons.

Takedown policy
Please contact us and provide details if you believe this document breaches copyrights.
We will remove access to the work immediately and investigate your claim.

This work is downloaded from Delft University of Technology.
For technical reasons the number of authors shown on this cover page is limited to a maximum of 10.

NeuroImage: Clinical 39 (2023) 103506

Contents lists available at ScienceDirect

NeuroImage: Clinical

journal homepage: www.elsevier.com/locate/ynicl

Quantitative MRI protocol and decision model for a 'one stop shop' early-stage Parkinsonism diagnosis: Study design

Samy Abo Seada [a], Anke W. van der Eerden [a], Agnita J.W. Boon [b], Juan A. Hernandez-Tamames [a,c,*]

[a] Department of Radiology and Nuclear Medicine, Erasmus MC, Rotterdam, The Netherlands
[b] Department of Neurology, Erasmus MC, Rotterdam, The Netherlands
[c] Department of Imaging Physics, TU Delft, The Netherlands

ARTICLE INFO

Keywords:
Atypical parkinsonisms
Parkinson
PSP
MSA
Quantitative MRI
Multi-modal
QSM
DTI

ABSTRACT

Differentiating among early-stage parkinsonisms is a challenge in clinical practice. Quantitative MRI can aid the diagnostic process, but studies with singular MRI techniques have had limited success thus far. Our objective is to develop a multi-modal MRI method for this purpose. In this review we describe existing methods and present a dedicated quantitative MRI protocol, a decision model and a study design to validate our approach ahead of a pilot study. We present example imaging data from patients and a healthy control, which resemble related literature.

1. Introduction

Parkinson's disease (PD) and other parkinsonisms are dominant and growing forms of neurodegenerative diseases (Poewe et al., 2017). Diagnosing atypical parkinsonism (AP) can be challenging due to the overlapping symptoms that patients present with during history taking and neurological examination. One in every four patients with atypical parkinsonisms initially receive an incorrect diagnosis (Hughes et al., 2002; Heim et al., 2017; Cozma et al., 2021). Patients with multiple system atrophy (MSA) (Poewe et al., 2022) and progressive supranuclear palsy (PSP) (Stamelou et al., 2021) are most often misdiagnosed. A British study (Hughes et al., 2002) showed that PSP is misdiagnosed between 24% and 59% of cases and a Finnish study (Joutsa et al., 2014) found a diagnostic sensitivity of 64.3% and 52.9% for MSA and PSP, respectively.

A correct diagnosis is important for patients to receive the appropriate treatment and guidance. There is currently no approved medication available, however clinical trials are ongoing (Cure PSP - clinical trials). If there are no red flags suggestive of PD (Marsili et al., 2018), the diagnosis of AP is commonly performed on clinical grounds only, without the need for an MRI scan. However Dutch and British (National Institute for Health and Care Excellence, 2017) clinical guidelines (Specialisten and Ziekte, 2020) recommend using MRI to aid the diagnosis of AP and rule out secondary parkinsonism (Ma et al., 2019). Conventional MRI has yet to show a clear clinical benefit for this task. Quantitative MRI techniques such as Quantitative Susceptibility Mapping (QSM) and Diffusion Tensor imaging (DTI) (Heim et al., 2017; Chougar, 2020; Lehericy et al., 2017; Pyatigorskaya, 2020; Bae et al., 2021) can improve the decision-making process but are yet to be investigated in large-scale studies.

While studies have shown that quantitative MRI biomarkers could improve clinical differentiation, a single MR-biomarker is unlikely to differentially diagnose PD, MSA and PSP with high accuracy. Recent studies have demonstrated diagnostic potential using multi-modal MRI and some have additionally proposed a form of multi-modal decision model (Pyatigorskaya et al., 2020; He, 2021; Leng, et al., 2022; Mangesius et al., 2020; Chougar et al., 2021; Jin, 2019). While most work on this topic is based on studies in patients with a clear diagnosis, the clinical relevance would be higher if such methods could differentiate between the diseases at an early stage, when the diagnosis is clinically unclear.

In this work we review existing methods, propose a multi-modal MRI decision model, and describe a study design for our pilot study. Our goal is to design a decision model based on multi-modal quantitative MRI

* Corresponding author at: Department of Radiology and Nuclear Medicine, Erasmus MC, Rotterdam, The Netherlands.
E-mail address: j.hernandeztamames@erasmusmc.nl (J.A. Hernandez-Tamames).

https://doi.org/10.1016/j.nicl.2023.103506
Received 30 March 2023; Received in revised form 21 June 2023; Accepted 4 September 2023
Available online 9 September 2023
2213-1582/© 2023 The Author(s). Published by Elsevier Inc. This is an open access article under the CC BY-NC-ND license (http://creativecommons.org/licenses/by-nc-nd/4.0/).

markers which predicts the final diagnosis in an early stage of the disease, when the clinical picture is an unclear form of parkinsonism, i.e. a clinically unclassifiable parkinsonism (CUP). The most appropriate classification model would be data-driven, trained with data from subjects who had a CUP at the time of scanning and tested on similar unseen subjects once the clinical diagnosis is clear. Recruiting a large cohort in this period of the disease is practically challenging. We propose two compromises, firstly to use decision rules with MRI-biomarkers that have been found to be significant in diagnosed patients, and secondly to train models using data from patients who received a recent diagnosis (within 5 years) and validate them in patients with CUP. Ultimately, our aim is to make such a decision model appropriate for clinical practice.

We reviewed the recent literature and considered the most promising biomarkers so far for differentially diagnosing PD, MSA and PSP patients. We propose a decision model which uses atrophy measurements in and around the brainstem (Oba et al., 2005; Nicoletti et al., 2006; Quattrone et al., 2008; Massey et al., 2013) and of the third ventricle (Quattrone et al., 2018), QSM markers (Mazzucchi, 2019; Sjöström et al., 2017), DTI markers (Du et al., 2017) and neuromelanin markers (Ohtsuka et al., 2014). We present a dedicated parkinsonism MRI protocol to acquire the necessary information.

To perform prediction at an individual level, cut-off values need to be determined for the individual decision rules. Considering the reported statistical significance, we estimate that a large cohort of about 150–200 CUP patients would be needed to train such a decision model. To justify such a clinical study, we propose to run a pilot study to investigate group differences for the decision rules in a small cohort of diagnosed and CUP patients. In other words, if group differences can be detected in a small cohort of CUP or diagnosed patients, it would motivate recruiting a larger cohort to predict patient outcome at an individual level.

We report on the background of biomarkers underlying the decision rules, and the rationale behind combining them. In-vivo images related to the biomarkers and decision rules are presented for a healthy control and patients.

2. Background and theory

In 2.1 a review of reported methods in the literature for differentiating PD, MSA and PSP with MRI is discussed. Two subtypes for MSA are considered, namely the cerebellar type (MSAc) and parkinsonian type (MSAp), and use the term MSA to imply both subtypes. Although many MR-based studies have been performed, there is no unequivocal method used in clinical practice for diagnosing MSA and PSP using MRI. Each subsection explains how the biomarkers are beneficial for our decision model (Fig. 1). Section 2.2 describes how the aggregate of information gathered by these methods can be used for differential diagnosis.

2.1. Review

2.1.1. Atrophy measurements

Promising techniques based on atrophy measurements have been proposed in the past which make use of atrophy measurements in the brainstem. Oba et al. (Oba et al., 2005) proposed a six-fold measurement of the midbrain and pons areas ($A_{midbrain}, A_{pons}$) to calculate their ratios and use the mean ratio. Nicoletti et al. (Nicoletti et al., 2006) demonstrated a reduction in the middle cerebellar peduncle (MCP) diameter in MSA patients. Quattrone et al. (Quattrone et al., 2008) built on these studies by proposing the Magnetic Resonance Parkinsonian Index (MRPI). They simplified the pons-to-midbrain ratio measurement (performing it only once) and added diameter measurements of superior

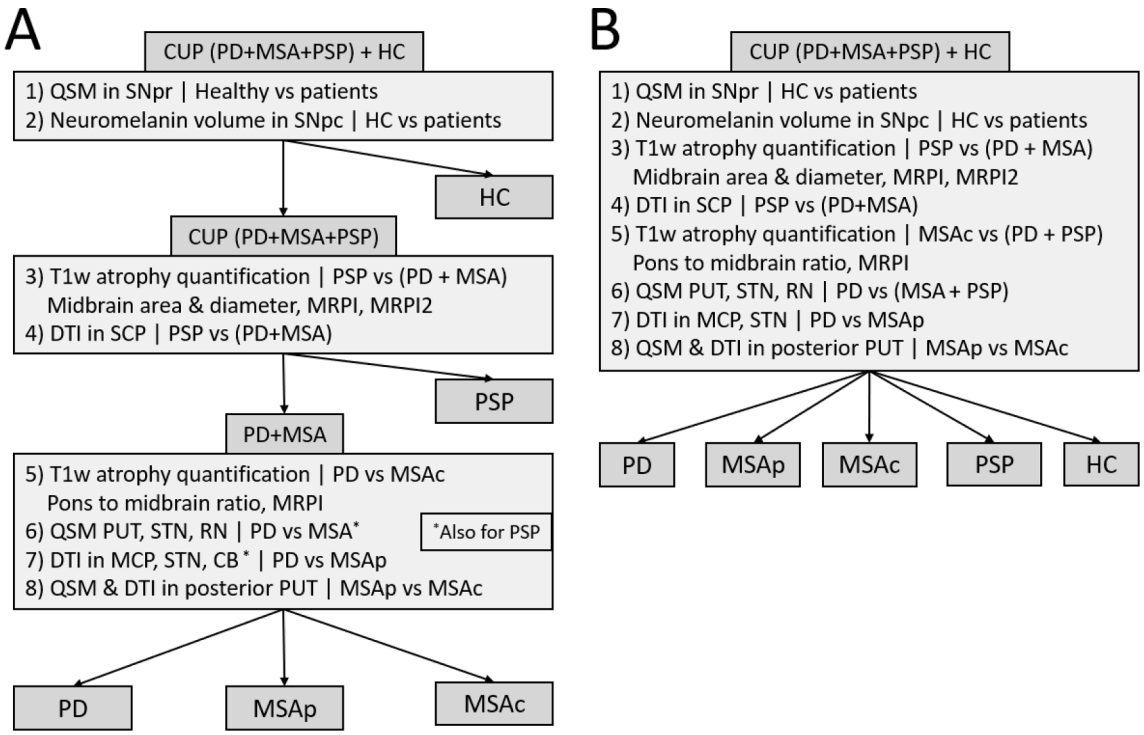

Fig. 1. Decision models for differentially diagnosing Parkinson's disease and other parkinsonisms. The decision tree in A is made up of up two binary classification followed by one multi-class classification. The cut-off values are weighted combinations of individual decision rules. Training such a decision model will require a cohort of 150–200 patients, which is outside the scope of our pilot study. (*) indicates metrics which overlap between MSA and PSP patients, and thus rely on separating PSP patients in the second stage. B shows an alternative model where all biomarkers are considered in a single multi-class classification. Decision rules 1–8 relate to the first column of Table 1, where the biomarkers and relevant study results are summarised. CUP: clinically unclassifiable parkinsonism. PD: Parkinson's disease. MSA: multiple system atrophy. PSP: progressive supranuclear palsy. HC: healthy controls. DTI: diffusion tensor imaging. QSM: quantitative susceptibility mapping. PUT: putamen. SCP: superior cerebellar peduncle. STN: subthalamic nucleus. RN: red nucleus. MCP: middle cerebellar peduncle. CB: cerebellum. SNpr: substantia nigra pars reticulata. SNpc: substantia nigra pars compacta.

cerebellar peduncles (SCPs). They multiplied the pons-to-midbrain ratio with the ratio of the mean diameters of the MCPs to the mean diameters of the SCPs measured on 3 consecutive oblique slices.

$$MRPI = \frac{A_{pons}}{A_{midbrain}} \times \frac{D_{MCP}}{D_{SCP}}$$

Massey et al. (Massey et al., 2013) proposed a simplified alternative approach to assess the pons-to-midbrain area relation with a ratio of the short axis diameter (D^{short}) of two ellipses, one ellipse covering the curvature of the pons (D^{short}_{pons}) and the other of the midbrain ($D^{short}_{midbrain}$). Quattrone et al. (Quattrone et al., 2018) later proposed MRPI2, which in addition to MRPI also uses atrophy around the third ventricle relative to the frontal horns.

$$MRPI2 = MRPI \times \frac{W_{3rd-ventricle}}{W_{frontal-horns}}$$

A shared result from these studies was that PSP was well differentiated from other cohorts, with high sensitivity (Table 1). This makes atrophy quantification from high-resolution T1-weighted images an interesting step for differentiating PSP from healthy controls (HC), MSA and PD (rule 3 in our decision model, Fig. 1)). Studies by Quattrone et al., which proposed MRPI and MRPI2, showed high accuracies for differentiating PSP from PD, however studies reproducing their performance has been more limited.

Mangesius et al. (Mangesius et al., 2018) compared the diagnostic performance of area and diameter measures as stand-alone biomarkers as well as incorporated these in MRPI in a retrospective and prospective study. Here a simplified version of MRPI was used, measuring the SCP diameter in a single oblique slice. They found the best results for the differentiation of PSP vs non-PSP using a decision tree only using D^{short}_{pons} / $D^{short}_{midbrain}$ and $D^{short}_{midbrain}$. The biomarkers tested did not perform as well for the differentiation between PD vs non-PD and MSA vs non-MSA.

Möller et al (Möller, 2017). found that $A_{midbrain}$, and $D^{short}_{midbrain}$ were both successful in differentiating PSP from HC, PD and MSA However, including MCP to SCP diameter ratios for MRPI performed less well, which was attributed to the difficulty in making measurements of the peduncles. A similar result was reiterated in a later meta-review article (Heim et al., 2021). It was also found that the pons-to-midbrain area ratio was lower in MSAc and MSAp compared to PD (rule 5 in our decision model) (Möller, 2017).

A large number of studies use automated brainstem segmentation software (Iglesias et al., 2015; Bocchetta et al., 2020) and verified that they can be used to obtain metrics to differentiate PSP from other groups using ROI-based methods (Bocchetta et al., 2020; Messina et al., 2011; Scherfler et al., 2016; Huppertz et al., 2016; Kim et al., 2022; Krismer et al., 2019). Furthermore, voxel-based approaches achieved high accuracies and can allude to relevant anatomies (Shao, 2014; Shao et al., 2015; Cui et al., 2020; Salvatore et al., 2014), and a recent deep learning approach achieved accuracies above 90% (Kiryu et al., 2019).

In conclusion, after reviewing the literature, we propose to investigate manual and automated measurements of the pons and midbrain, area and diameters (A_{pons}, D^{short}_{pons}, $A_{midbrain}$, $D^{short}_{midbrain}$), their ratios, MRPI and MRPI2 as potential biomarkers for differentiating PSP patients from others, and to differentiate PD from MSA.

2.1.2. Diffusion imaging

Diffusion imaging is an MR imaging technique which is sensitive to the random motion of watermolecules. Within this domain, Diffusion Tensor Imaging (DTI) requires strong diffusion in at least six directions and forms the basis for estimating fractional anisotropy (FA) and mean diffusivity (MD) (Stoessl et al., 2014). An overall reduction in FA can be interpreted as the loss of microstructural integrity of myelin around axons (Zhang and Burock, 2020). Abnormalities in the SN affect the dopaminergic output in the corticobasal ganglia-thalamocortical motor circuit, which together with the accumulation of lewy bodies are

Table 1
Summary of the statistical results from previous results used in a proposed decision model. (*) indicates that a biomarker overlaps for MSA and PSP, which is the case for some QSM and DTI biomarkers. For rules 1 and 2 popular qualitative markers are also mentioned.

Decision rule	Study and biomarker	Reported result (sensitivity/specificity) [N vs N]
1) SWI and QSM in SNpr Healthy vs patients	Sjöström 2017. QSM in SN (Fig. 1)	HC vs PD ($p = 0.030$) [14 vs 62]; HC vs PSP ($p = 0.002$) [14 vs 15]; HC vs MSA ($p = 0.032$) [14 vs 11]
	Cheng 2019. Swallow tail and QSM in SN (Text)	PD vs Healthy (89%/87%) [87 vs 77]
	Schwarz 2014. Swallow tail on SWI (Table 1)	PD vs non-PD patients (100%/95%) [9 vs 81]
2) NM MRI Healthy vs patients	Kashihara 2011. NM volume in SNpc (Text)	HC vs PD ($p < 0.001$) [54 vs 80]; HC vs PSP ($p < 0.001$) [54 vs 11]; HC vs MSA ($p < 0.001$) [54 vs 28]
	Ohtsuka 2014. Contrast ratio lateral SNpc. (Fig. 2A)	PD vs control $p < 0.0001$ with effect size 0.62 [30 vs 22] MSAp vs control $p < 0.01$ with effect size 0.52 [10 vs 22]
3) Atrophy quantification PSP vs (PD + MSA)	Quattrone 2018. MRPI2 (Table 2)	PSP-p vs PD cut-off-value 2.18 (100%/94.3%) [34 vs 53]
	Quattrone 2008. MRPI (Table 4)	PSP vs PD cut-off value 13.55 (100%/100%) [33 vs 108] PSP vs MSA cut-off value 12.85 (100%/100%) [33 vs 19]
	Möller 2017. MRPI (Table 2)	PSP vs PD cut-off 8.51 (68.9%/67.7%) [106 vs 204] PSP vs MSA-c cut-off 7.61 (92.5%/85.7%) [106 vs 21]
	Möller 2017. Midbrain area (Table 2)	PSP vs PD cut-off 124 mm^2 (84.0%/83.8%) [106 vs 204] PSP vs MSAp cut-off 117.0 mm^2 (78.3%/81.7%) [106 vs 60] PSP vs MSAc cut-off 114.0 mm^2 (74.5%/85.7%) [106 vs 21]
	Mangesius 2018. Midbrain diameter (Table 2)	PSP vs non-PSP cut-off 8.9 mm (90.0%/90.2%) [55 vs 257]
	Mangesius 2018. MRPI (Table 2)	PSP vs non-PSP cut-off 15.62 (82.9%/86.2%) [55 vs 257]
4) DTI in SCP PSP vs (PD + MSA)	Du 2017. DTI SCP and others (Table 2)	PSP vs PD (94%/94%) [19 vs 35] PSP vs MSAp (94%/92%) [19 vs 16]
	Nicoletti 2008. rADC in SCP (Table 2)	PSP vs (PD + MSAp) (100%/93.3%) [28 vs 30]
	Planetta 2016. Free-water DTI in SCP (Table 4)	PSP vs PD (100%/100%) [18 vs 18]
5) Atrophy quantification MSAc vs PD	Möller 2017. Midbrain/Pons area ratio (Table 2)	MSAc vs PD cut-off 0.290 (82.2%/83.2%) [21 vs 204]
	Möller 2017. MRPI (Table 2)	MSAc vs PD cut-off 6.22 (76.2%/88.8%) [21 vs 204]
6) QSM PD vs MSA	Mazzuchi 2019. QSM (Table 4)	PD vs MSA using Putamen, STN and RN. AUC:0.818, 0.808, 0.779 respectively [35 vs 12]
	Sjöström 2017. QSM (Fig. 1)	PD vs MSA using Putamen and RN. $p = 0.002$ and $p = 0.022$ respectively [62 vs 11]
7) DTI PD vs MSA	Du 2017. DTI indices (Table 3)	PD vs MSAp using FA in MCP, STN, CB (83%/86%) [35 vs 16]
	Worker 2014. DTI indices (Table 2)	PD vs MSA using FA in MCP ($p = 0.0021$) [14 vs 16]
8) Posterior Putamen MSAp vs MSAc	Chougar 2023. MD values (Table 2)	MSAc vs MSAp using MD in posterior putamen ($p < 0.001$) [6 vs 21]
	Chougar 2023. R2* values (Table 2)	MSAc vs MSAp using R2* in posterior putamen ($p < 0.001$) [6 vs 21]

accompanied with demyelination of white matter bundles (Zhang and Burock, 2020). Several studies investigated changing DTI metrics in PD (Langley et al., 2016; Schwarz et al., 2013).

Du et al. (Du et al., 2017) studied the combination of R2* and DTI indices in AP and found that DTI changes in the SCP were unique to PSP patients, while changes in the MCP and subthalamic nucleus (STN) were unique to MSAp patients. Worker et al. (Worker et al., 2014) also found MCP changes in MSA patients. Changes were also found with a more advanced diffusion model known as free-water DTI (Pasternak et al., 2009). Planetta et al. (Planetta et al., 2016) found significant changes using free-water DTI in the SCP for PSP patients, but no changes appeared unique to MSA patients. Both studies found cerebellum (CB) changes for MSA and PSP patients. Two recent reviews (Chougar, 2020; Bae et al., 2021) found that DTI could not perform the differentiation on its own, while two studies found that using only DTI features achieved high accuracies when combined with machine learning analysis (Talai, 2021; Archer et al., 2019). More advanced diffusion models such as NODDI have shown similarly high accuracy as free-water DTI (Mitchell et al., 2019).

In conclusion, we propose to investigate FA measures in the SCP to differentiate PSP from PD and MSA, and to use FA in the MCP, STN and white matter of the CB to differentiate PD from MSA (rules 4 and 7 respectively in our decision model). More complex DTI models could be explored.

2.1.3. Iron imaging

Common iron-sensitive MR imaging techniques are, in increasing post-processing complexity, R2*-mapping, susceptibility-weighted imaging (SWI) (Meijer et al., 2016; Meijer et al., 2015) and Quantitative Susceptibility Mapping (QSM). R2* and QSM are both quantitative techniques and QSM has been found to be more sensitive than R2* to changes in iron concentration for PD patients (Langkammer et al., 2016). PD, MSA, and PSP patients all show iron accumulation in the SN, making it a useful biomarker for differentiating healthy subjects (rule 1 in our decision model). However, which iron-sensitive markers best aid the differential diagnosis of AP patients has been an outstanding question.

Meijer et al. (Meijer et al., 2016; Bae et al., 2016) investigated R2* and SWI in the SN for AP differentiation and reported high specificity yet low sensitivity. Similarly, Mazzucchi et al. (Mazzucchi, 2019) evaluated QSM in the SN and found no group differences among PD, PSP and MSA, however they did find differences between PD and both MSA and PSP in the red nucleus (RN), STN and the putamen (PUT). Sjöstrom et al. (Sjöström et al., 2017) found a similar pattern of susceptibility differences in the RN for MSA and PSP, and changes in the PUT for MSA, while Du et al. (Du et al., 2017) also found elevated R2* in the STN for MSAp patients and in the posterior SN for PSP patients.

SWI, R2* and QSM are useful biomarkers for identifying healthy subjects (rule 1 in our decision model), and in addition could be a helpful marker for the differential diagnosis of PD and AP, however there is an overlap between susceptibility values for both MSA and PSP patients. We hypothesise that QSM could play an important role for differentiating PD from MSA and PSP (rule 6 in our decision model) and PD from MSA, if PSP can be separated from MSA using other markers. In conclusion, we will investigate QSM values in deep nuclei and basal ganglia structures in our decision model.

2.1.4. Neuromelanin imaging

Neuromelanin (NM) is a dark pigment primarily found in the substantia nigra pars compacta (SNpc) and locus coeruleus (LC). The pigment consists of organic compounds as well as metal ions, such as iron (Trujillo et al., 2017). Imaging neuromelanin with MRI is possible in several ways, commonly with either magnetization transfer (MT)-weighted gradient-echo or T1-Fast Spin Echo (FSE) sequences. The hyperintense contrast from NM-MRI is attributed to a combination of MT and (mainly) T1-shortening effects due to the iron present in NM pigments (Trujillo et al., 2017). In MT-weighted gradient-echo sequences, MT-weighting is achieved by saturating the protons in the bound pool using dedicated MT-pulses prior to selective excitation. For T1-FSE sequences, refocusing pulses at short inter-echo times have a similar saturation effect to the bound pool (Priovoulos et al., 2018), albeit indirectly. In both cases T1-weighting can be achieved by using short echo-times, which is why both sequence families are eligible for NM-MRI.

An advantage of this imaging technique is that it requires no further post-processing unlike QSM and DTI. Neuromelanin concentration decreases in patients with parkinsonism (Kashihara et al., 2011), and studies typically analyse signal intensity changes (Ohtsuka et al., 2014; Isaias, 2016) or volume measurements (Ogisu et al., 2013; Oshima, 2021; Takahashi, 2018). Several studies have shown its usefulness in the diagnosis of idiopathic Parkinson's disease (Ohtsuka et al., 2014; Ogisu et al., 2013; Sasaki et al., 2006; Sulzer, 2018). NM changes related to different AP conditions is unclear (Ohtsuka et al., 2014; Simões et al., 2020) and its usage in AP differentiation is yet to be investigated (Lehericy et al., 2017; Bae et al., 2021; Pavese and Tai, 2018).

In conclusion, performance for differential diagnosis of AP based on NM-MRI is arguable but worthy of further investigation. One advantage is to use SNpc volume measurements to eliminate healthy controls from all parkinsonisms (Kashihara et al., 2011) (rule 2 in our decision model). In our study we will evaluate SNpc volume using manual and automatic segmentation (Gaurav, 2022). In addition, CNR in the LC will be investigated (Isaias, 2016), however how this can be reliably quantified is an outstanding question.

2.2. Differential diagnosis

In this section we will propose how, based on the conclusions in 2.1, a differential diagnosis could be made combining data obtained with atrophy imaging, neuromelanin-MRI, iron-sensitive imaging, and diffusion imaging. Key to the design of this decision model are three insights:

- All forms of parkinsonisms show elevated iron in the SNpr and neuromelanin reduction
- Atrophy quantification is a reliable test to separate PSP from other diseases
- QSM and DTI metrics for MSA and PSP patients largely overlap with each other, but in certain structures show significant differences from PD patients

We propose two decision models which could complement each other. One model is a decision tree, which is presented in Fig. 1A. The other is a single multi-class classification model, which is presented in Fig. 1B. Both models use a total of 8 decision rules, and classification should be performed with a probabilistic output to adhere to the complex nature of these diseases (Chougar et al., 2021; Wenning et al., 2022). Statistical performances from relevant publications are summarised in Table 1, categorised for each decision rule.

The decision tree in Fig. 1A is made from two stages of binary classification followed by one stage of multi-class classification. In the first stage, we assume the subject can be either a PD, PSP or MSA patient, or HC. Healthy controls are separated from patients using iron-sensitive and neuromelanin MRI. In the second stage, PSP patients are separated from PD and MSA using a combination of markers unique to PSP, namely atrophy quantification (Quattrone et al., 2008), and DTI on the SCP (Du et al., 2017). In the third stage PD, MSAp and MSAc are differentiated using atrophy, QSM and DTI. From these, the reduced FA markers derived from the MCP and STN are unique to MSAp patients, while FA reduction in the CB is common for both MSAp and PSP. QSM metrics on the other hand are increased in the PUT, STN and RN for both MSA and PSP patients, compared to healthy controls and PD patients. Therefore, a correct classification in the third stage based on these

markers relies on the correct classification in the second stage. Another reliable test for PD vs MSAc can be made based on atrophy, using pons-to-midbrain area ratios and MRPI (Möller, 2017), while the subtypes of MSAc and MSAp can differentiated by using QSM and DTI markers in the posterior putamen (Chougar, 2023).

A benefit from a decision tree with handpicked rules is its simplicity and traceability for differential diagnosis. However, misclassification in early rules have knock-on effects on the overall performance, and it is difficult to decide how to incorporate additional biomarkers when the classification confidence is low. For example, PSP can be expected to be misclassified about 10–20% based on atrophy which violates the assumption in rules 6 and 7 (Chougar, 2023; Möller, 2017), in which case it could be beneficial to consider other markers from other rules. Thus, an alternative approach is to perform a single multi-class classification with all the decision rules (Fig. 1B), using a classifier which copes well with high-dimensional data such as support vector machines.

We opt not to differentiate between the two different forms of PSP (PSPp and PSPrs) since there is an insufficient amount of research of quantitative MRI techniques for these tasks, and the possible clinical management is not significantly affected with improved subtyping (Bluett, 2021).

3. Study design and methods

3.1. Study objectives and design

The decision models in Fig. 1 could be clinically valuable to predict patient outcome at an individual level. However, training such models would require a large cohort scanned with a dedicated MRI protocol. To justify a large clinical study based on the proposed decision tree, it would be important to have preliminary data showing group differences for its decision rules.

The objective of our pilot study is to investigate whether a quantitative MRI protocol and quantitative post-processing can detect group differences for the decision rules proposed in the decision tree. We will compare this data between patients whose diagnoses were clinically unclear (CUP) at the time of scanning, and will likely be diagnosed with either PSP, MSA or Parkinson's disease within 12 months. The final analysis will be performed after all patients have received their diagnosis from an experienced neurologist. We will also include diagnosed PD, PSP, MSAp and MSAc patients to investigate group differences for the decision rules between the diseases, as well as between the CUP and diagnosed patients.

Patients and controls will be informed and recruited for the study as described below, and after signing informed consent forms will receive an MRI within approximately 6 weeks. Patient participants with an uncertain diagnosis will receive an MRI as part of their clinical management, with additional quantitative MRI series. All other participants will receive an identical MRI exam.

3.2. Population

Patients will be recruited from the outpatient movement disorder clinic at Erasmus MC in Rotterdam, the Netherlands. Inclusion criteria for all patients is that they present with symptoms consistent with early degenerative parkinsonism and are at least 50 years old. In addition, there should be a reason to suspect the patient from another diagnosis than PD, because of at least one red flag for PD, but without symptoms or signs pointing to one specific atypical parkinsonism (National Institute for Health and Care Excellence, 2017).

Inclusion criteria for diagnosed PSP, MSA and PD patients is that their diagnosis is highly suspected and the onset of disease is below 5 years. All subtypes of PSP and MSA will be considered and included.

Exclusion criteria for all patients are parkinsonism symptoms caused by medication or essential tremors, a history of another neurodegenerative disease or significant intracranial disease (in line with Fazekas 3), pregnancy or lactation, or any physical or mental status that interferes with the informed consent procedure.

This work is exploratory in nature, and we anticipate that a minimum of 30 CUP patients are needed to evaluate the importance of the decision rules at an disease stage. We will also recruit age-matched healthy volunteers between the age of 50 and 75. The healthy volunteers as well as the diagnosed patients will serve as reference data for the quantitative MRI techniques. We anticipate that a minimum of 10 participants per group (PD, PSP, MSAp and MSAc, healthy control) are required. Since this is a pilot study with a relatively small group of participants we have not performed statistical power calculations.

Within 12 months, all participants are contacted for a follow up. For undiagnosed patients, this will occur simultaneously with a hospital visit as part of their regular clinical management. For patients who already received a diagnosis at recruitment, the goal of follow-up is to confirm their diagnosis remains unchanged. For healthy controls, the follow-up is by telephone to ensure they have not developed any parkinsonian symptoms or other neurological disorder.

3.3. Clinical examination

Both at baseline and at 12 months follow-up the patients will undergo a clinical examination by a neurologist, including general information (age, gender, age at onset, disease duration) as well as motor signs at onset using UPDRS-III. Functional assessment is made with a H&Y score and a cognitive assessment with MOCA. The examinations are video recorded for further examination.

3.4. MRI acquisition and post-processing

The proposed protocol includes a 2D T2-weighted propeller FSE, a 3D high-resolution T1w-SPGR, a 3D multi-echo gradient-echo sequence for SWI and a 2D MT-weighted gradient-echo sequence and a DTI sequence. Data is acquired on a GE 3T Signa Premier (GE healthcare, Chicago, USA) equipped with a 48-channel head-coil. Acquisition details are summarised in Table 2.

The study and MRI protocol were approved by the local ethics committee, and informed consent was acquired from all participants prior to the MRI scan. For the example results in this article, QSM images were produced from the raw data of the SWI sequence. QSM processing steps such as phase unwrapping (Liu et al., 2013; Kressler et al., 2010; de Rochefort et al., 2008); background field removal (Liu et al., 2011; de Rochefort et al., 2010) and dipole inversion (Liu et al., 2013) were performed using the MEDI toolbox.

Single-shell DTI was acquired with a b-value of 1000 in 64 directions and 10 images with a b-value of 0. A separate sequence with reversed phase-encoding directions was acquired to retrospectively correct for susceptibility-induced distortions (Andersson et al., 2003). Correction for eddy currents was performed (Andersson and Sotiropoulos, 2016) and Fractional-Anisotropy was calculated using FSL *dtifit*.

Neuromelanin-MRI was acquired using a 2D gradient-echo sequence with MT-weighting (Chen et al., 2014; Wengler, 2021). During setup we experimented with T1-FSE (Isaias, 2016) and 3D gradient-echo (Ogisu et al., 2013). However, our final choice showed better NM contrast during piloting, in agreement with other reports (Sulzer, 2018; van der Pluijm et al., 2021). Partial Fourier was disabled in the readout direction since it gave improved SNR results and resilience to susceptibility, without affecting neuromelanin contrast. In addition to our study outcomes, T1 and T2-weighted and other structural images are used for excluding secondary parkinsonisms (Ma et al., 2019).

3.5. Outcome measures

Our outcome measures will report on all group differences for the decision rules of the proposed decision models (Fig. 1). An outline is as following:

Table 2
Acquisition sequence details used for a dedicated parkinsonism protocol. Voxel size [Frequency resolution, phase resolution, slice-thickness in mm]; Matrix size = [Frequency × Phase × Number of slices] TE:echo-time [ms] TR: repetition-time [ms];FA: flip-angle [degrees];ACC: phase acceleration, SMS: simultaneous multi-slice; Acq time: Acquisition time [minutes:seconds]. Dir's: diffusion directions. MT: magnetization transfer. Rev pe: Separately acquired acquisition with reverse phase-encoding direction, used for distortion correction.

Sequence	Voxel size	Matrix size	TE	TR	FA	ACC	Other	Acq time
T1w-MPrage	0.9 × 0.9 × 0.9	256 × 256 × 176	3.2	8.1	12	2	3D	5:09
T2-Propeller	0.6 × 0.6 × 3	384 × 384 × 44	148	5536	160	2	2D	2:24
SWI / QSM	0.7 × 0.7 × 1	320 × 320 × 88	13:3.5:37.6	38.5	5	2	3Dunipolar	5:42
DTI	1.75 × 1.75 × 2	128 × 128 × 56	77.9	3138	90–180	SMS2 + 2	64 dir'sb1000	3:55 & 0:54 (rev pe)
NM-MRI	0.4 × 0.4 × 3	512 × 512 × 12	7.5	340	50	No Acc	3 repsMT: 8 ms 1200 Hz	7:28

1. HC vs (PD, PSP, MSA) with QSM in SNpr (and qualitative swallow tail sign)
2. HC vs (PD, PSP, MSA) with NM-MRI volume in SNpc (and LC quantitative CNR and qualitative score).
3. PSP vs (PD, MSA) with atrophy quantification including pons and midbrain area and diameters, pons-to-midbrain ratio, MRPI and MRPI2.
4. PSP vs (PD, MSA) with DTI-metrics in the SCP.
5. PD vs MSAc with atrophy quantification including pons and midbrain area and diameters, pons-to-midbrain ratio, MRPI and MRPI2.
6. PD vs MSA with QSM in Putamen, STN and RN.
7. PD vs MSAp with DTI metrics in MCP, STN, and white matter of CB.
8. MSAc vs MSAp with QSM and DTI metrics in the posterior PUT.

Where MSA is used, we combine MSAp and MSAc subjects where possible. For decision rules 1 and 2 we will investigate qualitative markers even if they will not fit in our overall quantitative approach. Any other patterns of interest will also be reported.

4. Preliminary results

The following results show illustrative examples of the type of images which will be used to analyse group differences for the proposed decision rules in Fig. 1. Fig. 3 shows T1-weighted images, where midbrain atrophy can be measured, for a healthy control (62 year female) and a MSA, PD and PSP patient (2 females, 64–66 years old). Fig. 3D and 3L shows visible atrophy for the PSP patient compared to the others. These images can be used for decision rule 3 for differentiating PSP from other groups, and for decision rule 5 for differentiating PD from MSA.

Fig. 4 shows neuromelanin-MRI from a healthy control and three patients, around the substantia nigra and locus coeruleus. Reduction of NM-contrast around the substantia nigra pars compacta seems clear for all patients compared to the healthy control, which could aid differentiating healthy controls from patients in decision rule 2. The LC is best visible for the healthy control, and its visibility is further reduced for all but the MSA patient. The small size of the LC and the low SNR and CNR associated with imaging it makes the hyperintense signal from the LC region an unreliable marker for differential diagnosis.

Fig. 5 shows QSM reconstructions from SWI data in three different views. High susceptibility values can be seen in the substantia nigra of all patients (Fig. 5b,c, d) compared to the healthy control (Fig. 5d), which is useful in decision rule 1. The SN pars reticulata of the MSA patient seems to have high susceptibility (red arrows, Fig. 5b). In the middle and bottom rows, the red nucleus and subthalamic nucleus respectively show that the susceptibility in the STN is higher in the MSA patient compared to the others. This could be useful in decision rule 6 to differentiate PD from MSA and PSP. The red nucleus is not visibly different between the PD and MSA patient. Fig. 6 shows QSM reconstructions at two levels of the basal ganglia. The marker of interest here is the susceptibility of the putamen, which is expected to be higher in MSA patients and is used in decision rule 6.

Fig. 7 shows Fractional Anisotropy (FA) maps derived from DTI data at three different views. MSAp patients are expected to have reduced FA in MCP compared to PD patients, as well as healthy controls, however this is not obvious from the example presented. Similarly, FA in the superior cerebellar peduncles of PSP patients is expected to be reduced. These metrics could be used in rule 7 for differentiating between PD and MSA, as well as decision rule 4 for differentiating PD and MSA from PSP.

5. Discussion

Atypical parkinsonisms (AP) are difficult to identify and differentiate from Parkinson's disease (PD) in the early phase of the disease, which results in high rates of misdiagnosis (Poewe et al., 2017; Hughes et al., 2002; Heim et al., 2017; Poewe et al., 2022). Conventional MRI biomarkers do not offer high sensitivity for clinical use in this phase. Studies using quantitative MRI have shown promising results, but a single technique to differentially diagnose among PD, MSA and PSP has not been found. We present a review of existing methods on the use of MRI for this task (Table 1), and propose a multi-modal decision model (Fig. 1) with 8 decision rules derived from existing literature, and present an MRI protocol to gather the right information (Table 2).

Our proposed acquisition protocol was optimized locally as a dedicated parkinsonism protocol. T1w images at high-resolution seemed

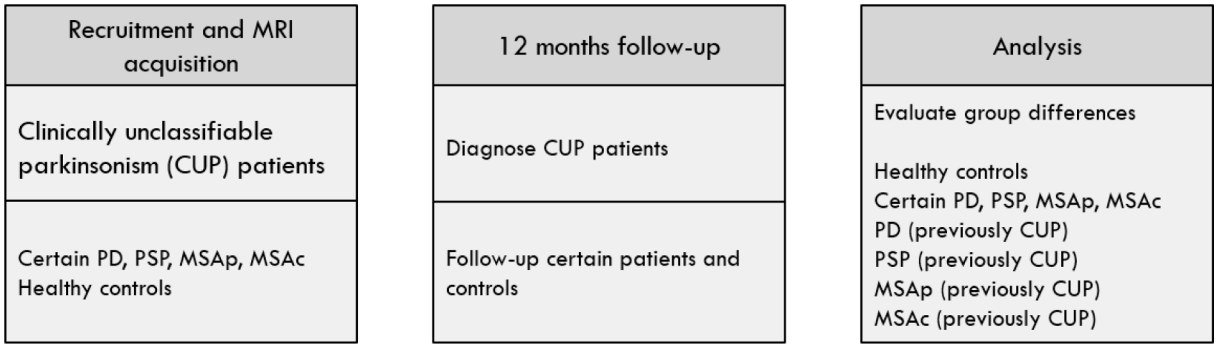

Fig. 2. Time-line of study design. Group differences will be analysed for the 6 groups shown in the right column.

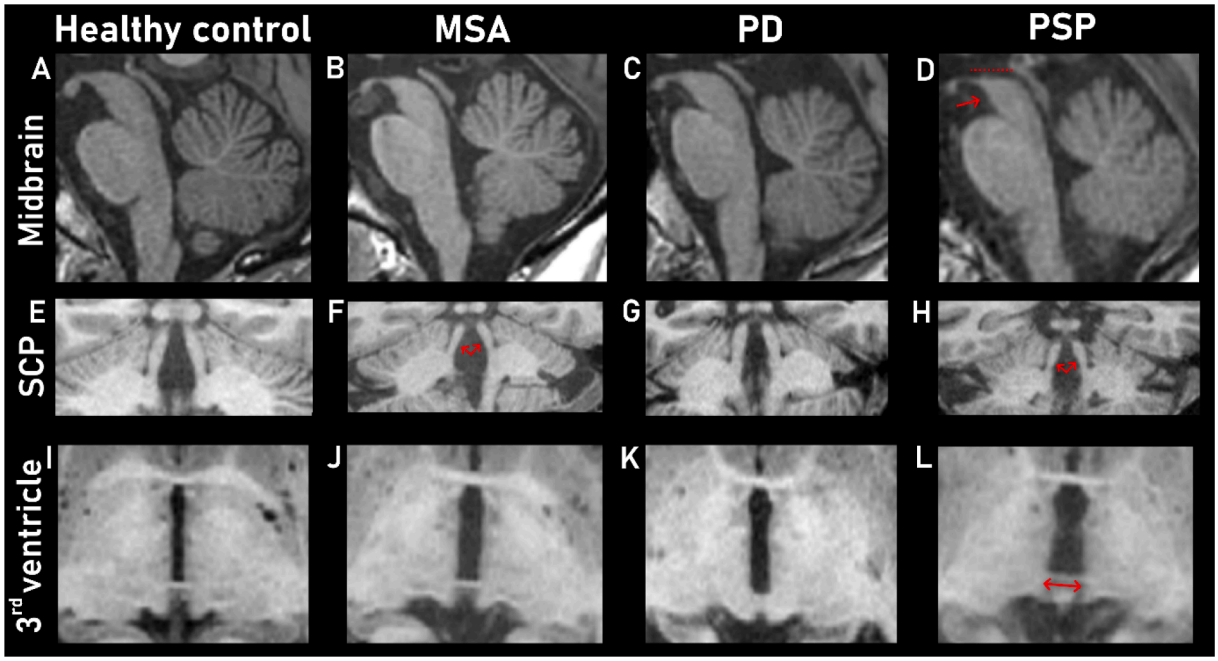

Fig. 3. T1-weighted images from a single series in a midsagittal view (a-d) that show the midbrain of a healthy control, multiple system atrophy (MSA), Parkinson disease (PD) and progressive supranuclear palsy (PSP) patient respectively. The PSP patient in D shows midbrain atrophy, and loss of the usual convex shape (red markings). The middle row (e-h) shows obliqued slices for measuring the diameter of the superior cerebellar peduncles (SCP, red arrows), which is expected to be reduced in the PSP patient. The bottom row (i-k) shows atrophy around the third ventricle (i-l) where atrophy in the PSP and MSA patient seems visibly higher. These images are intended for illustration and as such images of the frontal horns and MCPs are omitted. (For interpretation of the references to colour in this figure legend, the reader is referred to the web version of this article.)

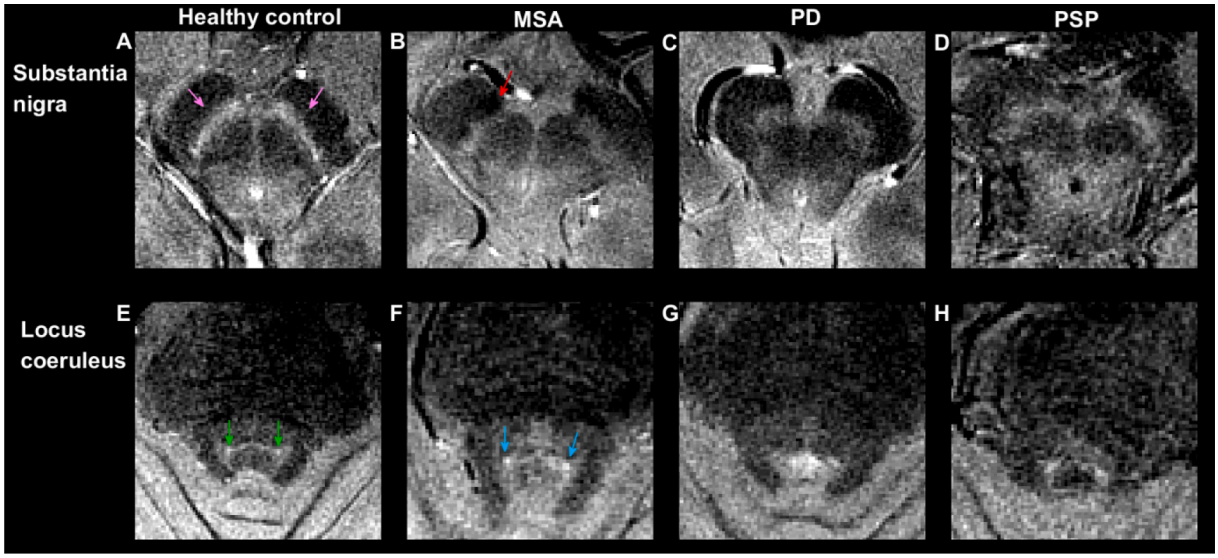

Fig. 4. Neuromelanin-MRI results from a healthy control, an MSA, PD and PSP patient. Neuromelanin appears hyperintense. Top row (a-d) shows a slice at the level of the substantia nigra for a healthy subject with neuromelanin mostly in the substantia nigra pars compacta (pink arrows) and NM area reduction of all patients (b-d). The MSA patient (b) has a hypointense region in the region of the substantia nigra pars reticulata (red arrow), which could be due to a high amount of iron in that region as visible in Fig. 5b. The bottom row (e-h) shows axial slices at a level where the LC seems best visible in the healthy subject (green arrows), but reduced in all patients, except the MSA patient (light-blue arrows). The small size of the LC and the low SNR and CNR associated with imaging it makes the hyperintense signal from the LC region an unreliable marker for differential diagnosis. (For interpretation of the references to colour in this figure legend, the reader is referred to the web version of this article.)

particularly relevant for measuring the superior cerebellar peduncles, and high in-plane resolution for the NM sequence seems important for visualising the locus coeruleus. The T2w image could alternatively be acquired with a 3D sequence, which could improve registration methods. A study found that approximate isotropic resolution was pertinent for reliable QSM estimation (Karsa et al., 2019). We chose an isotropic in-plane resolution which was higher than the slice-thickness, to improve delineation of deep nuclei within a clinically feasible acquisition time. For the sequence DTI we desired high in-plane resolution to visualise the cerebellar peduncles, however thin slice-thickness resulted in an unfavourable SNR reduction. We did not investigate the benefit of isotropic voxels and additional b-values, which could improve

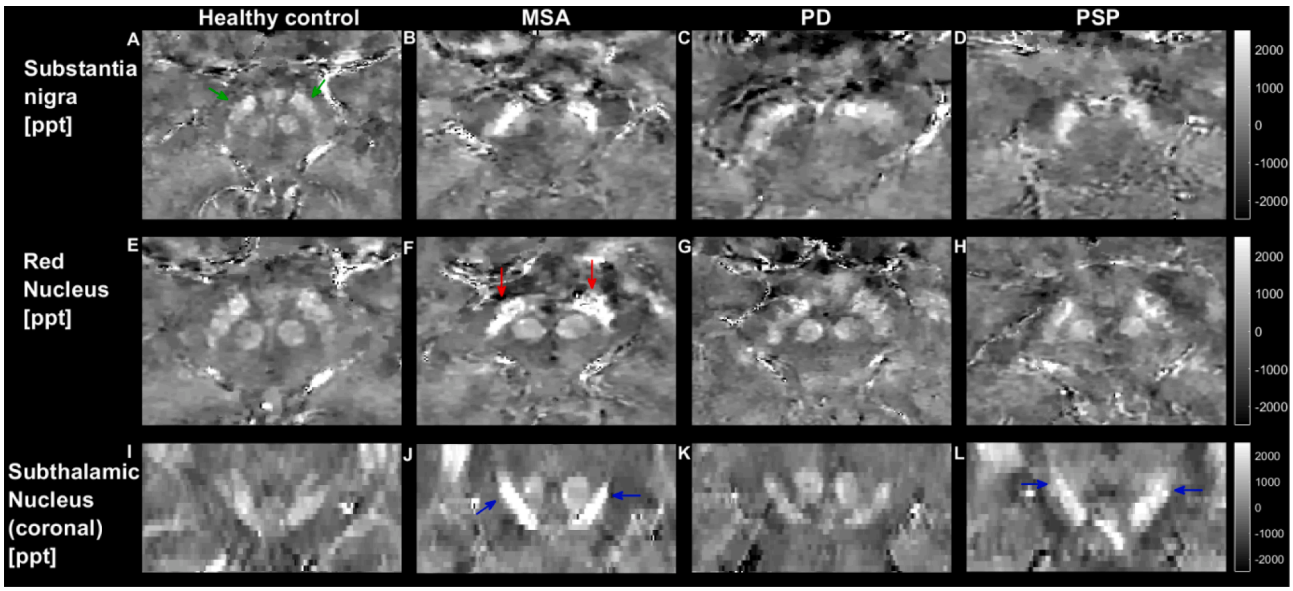

Fig. 5. QSM examples at three levels (top: axial, substantia nigra, middle: axial, red nucleus, bottom: coronal, subthalamic nucleus). All windows levels are equivalent (ppt: parts per trillion). High susceptibility values (displayed as high signal intensity) can be seen in the substantia nigra of all patients (b,c,d) compared to the control (a, green arrows), and in particular for the MSA patient (b). A slice through the red nucleus also shows higher susceptibility in the subthalamic nucleus at that level of the MSA patient (f, red arrows) compared to the other patients and healthy control. However, the susceptibility of the RN itself seems similar in all subjects. The subthalamic nucleus is better seen on a coronal slice (i-l) where the MSA and PSP patients both have higher iron content than the PD patient and healthy control (blue arrows), which could be useful to distinguish MSA from PD in decision rule 6. (For interpretation of the references to colour in this figure legend, the reader is referred to the web version of this article.)

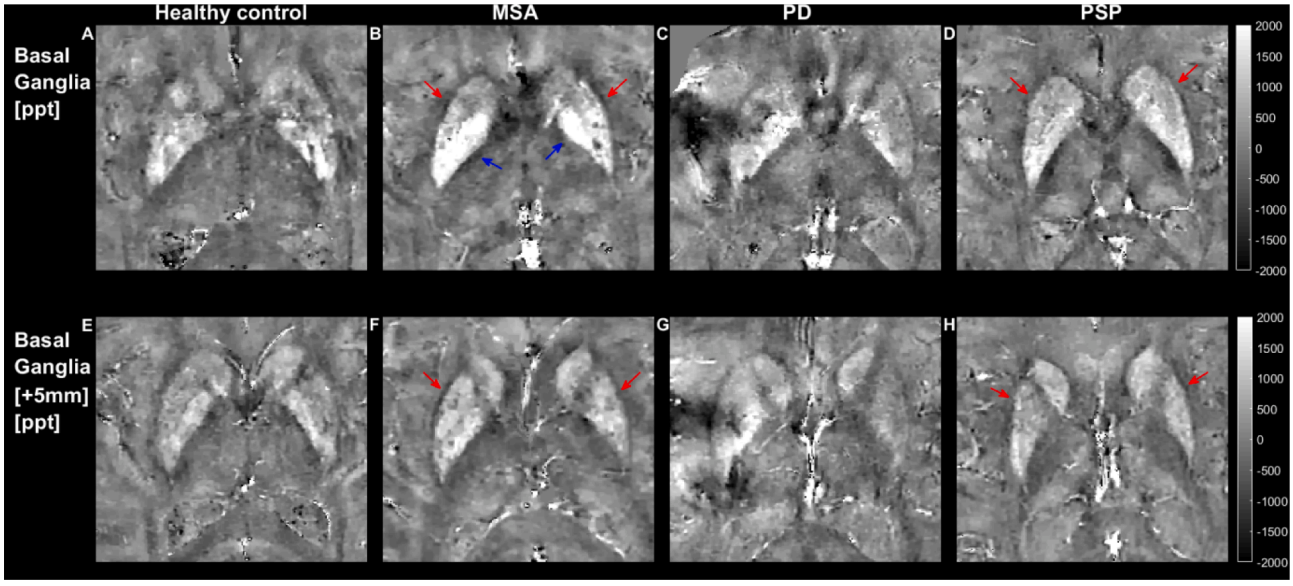

Fig. 6. Axial QSM images at upper and lower levels of the basal ganglia separated by 5 mm. All window levels are consistent. Most notably, the MSA and PSP patients show a higher amount of iron in the putamen (red arrows) than the healthy control and PD, which could be useful to distinguish MSA from PD in decision rule 6. In addition, the MSA patient shows high susceptibility in the globus pallidus (B, blue arrows). The QSM reconstruction for the PD patient contains a strong artifact. (For interpretation of the references to colour in this figure legend, the reader is referred to the web version of this article.)

DTI analysis.

The ultimate purpose of the decision model is to predict patient outcome at an early stage of the disease, however for this pilot study we merely want to investigate group differences in the populations of interest. We also present example results using the proposed MRI protocol and post-processed data. We share these results for illustrative purposes and stopped short of sharing actual quantitative measures as it would need more patient data.

Our general approach is a process of elimination to include markers specific to neurodegenerative parkinsonism, followed by markers specific to PSP, and finally markers which can separate PD and subtypes of MSA. The three key insights which support this approach (Section 2.2) are firstly, iron build-up and neuromelanin reduction in all parkinsonian disorders, secondly a unique pattern of midbrain, cerebellar and ventricular atrophy in PSP patients, and thirdly increased iron build-up in deep gray matter nuclei for MSA and PSP patients compared to PD.

Decision rule 1 aims to differentiate healthy controls from patients based on SWI and QSM in the SN (Fig. 5). SWI can be scored visually

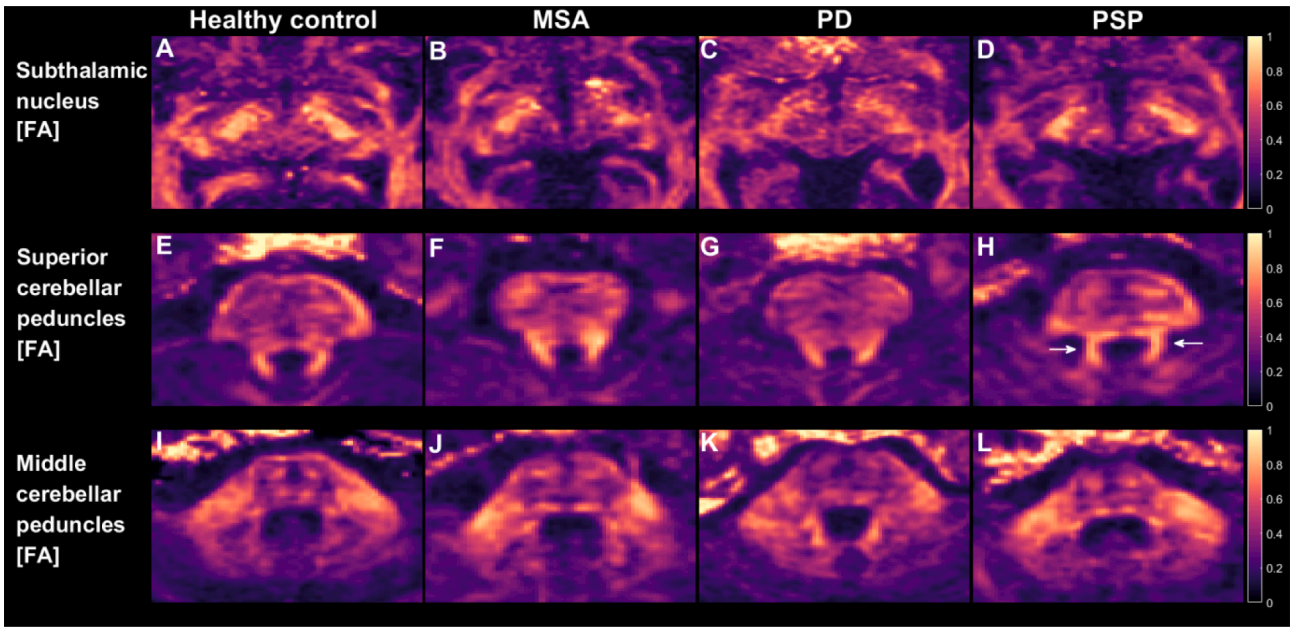

Fig. 7. Fractional Anisotropy (FA) maps from a healthy control, and an MSA, PD and PSP patient. All window levels are consistent. The top row shows axial slices at the level of the STN (the nucleus itself is not visible on FA), where it is expected that MSA patients will have a reduced FA. The middle row shows axial slices depicting the superior cerebellar peduncles, which are reported to show an FA reduction for PSP patients. The bottom row shows middle cerebellar peduncles, which are reported to show an FA reduction in MSAp patients compared to PD. None of the expected FA reductions seem visually appreciable.

with the loss of the swallow tail sign, while QSM is a quantitative technique which could be used in an automatic fashion. Several studies have investigated the use of SWI and QSM on the nigrosome for the AP differentiation task, with limited success (Meijer et al., 2016; Meijer et al., 2015). Decision rule 2 aims to differentiate healthy controls based on neuromelanin volume measurements in the SNpc (Fig. 4) manual or automatic segmentation (Gaurav, 2022). For the LC, visual scoring or contrast-to-noise ratios (CNR) measurements will also be considered (Isaias, 2016).

Decision rule 3 aims to differentiate PSP from PD and MSA using atrophy measures (Fig. 3), namely in the mid-sagittal view about the brainstem and axially where the third ventricle is at its widest. The PD and MSA patient also show increased ventricular atrophy compared to the healthy control. Although visual assessment can be done, making measurements is relatively straight-forward and allows for automatic techniques (Bocchetta et al., 2020; Scherfler et al., 2016; Kim et al., ; Krismer et al., 2019). There is also evidence that DTI-metrics in the SCP are unique to PSP patients, and decision rule 4 is based on this quantitative MRI technique (Fig. 7E-H).

Decision rules 5 to 7 propose to use atrophy, QSM and DTI to differentiate PD from MSA and its subtypes. Elevated QSM values can be seen in the STN and putamen of the MSA and PSP patient (Fig. 5I-L and Fig. 6), which after PSP differentiation can be used for separating MSA from PD. MSAc and MSAp can be separated using pons and MCP atrophy quantification, and by DTI and QSM metrics in the posterior putamen (decision rule 8).

An alternative approach to the decision tree in Fig. 1A is to use a single multi-class classifier with all the data (Fig. 1B). This reduces traceability compared to a decision tree, but allows the model to use all information available. Ideally one would learn decision rules from data collected from CUP patients, however due to the rarity of the diseases, acquiring this data is challenging. When using biomarkers that were significant in diagnosed patients, we are assuming that CUPs will show similar biomarker changes. This is likely not true, or some biomarkers will be more significant in early-stage classification, which is something a single-stage multi-class classifier would cope with better than a decision tree when trained on data from CUP patients.

A common issue with quantitative MRI in the clinic is variable performance across medical centers, which is down to the having the right expertise (Wang et al., 2017) and interpreting the results. A recent guide to practical MRI and PET/SPECT imaging methods in PD vs AP differentiation (Peralta et al., 2022). Broadly speaking, their MRI algorithm uses three phases: firstly to rule out secondary causes of parkinsonism, secondly to determine a degenerative form of parkinsonism, and thirdly to differentiate among PD, MSA and PSP using a combination of T1-weighted atrophy, diffusion imaging and to a lesser extent NM-MRI and SWI. Our first two decision rules fit well in the second phase, while the latter rules fit well in the third phase of this decision method. To facilitate future clinical implementation, we have opted for relatively standard QSM and DTI acquisition and reconstruction pipelines which showed significant differences between AP patients in previous studies.

QSM has relatively high inter-vendor reproducibility (Deh et al., 2015) but low reproducibility when using different reconstruction algorithms (Santin, 2017). Relatively simple DTI metrics have high inter-vendor reproducibility (Min et al., 2018), in particular FA, for which the FSL toolbox is a widely used reconstruction method. Care must be taken however, as a reduction in FA can also be caused by crossing white matter fibers. New DTI methods such as multi-shell DTI (Kamagata et al., 2018) or multi-dimensional DTI (Topgaard, 2017) could be more sensitive to microstructural changes. While promising and interesting, they require more design parameters, such as the number of b-values or diffusion trajectory, and number of directions of each. This can further complicate standardization for clinical use. Another avenue for exploration would be to report relative FA metrics, taking an unaffected white matter region as a reference value.

A possible outcome from this study could be that atrophy and only either QSM or DTI biomarkers are sufficient, which would be important knowledge for a follow-up clinical study and clinical translation. A recent similar multi-modal approach (Leng et al., 2022) found accuracy rates above 95% for diagnosed PD vs MSA, and PSP vs MSA using T1-weighted and DTI-based features alone. Our study will investigate patients in an earlier phase of their disease for higher clinical relevance. Neuromelanin-MRI is a well-researched MRI technique for Parkinson's disease, but has not proven successful so far in diagnosing atypical parkinsonisms. We aim to investigate if NM techniques are useful in early-stage patients.

In this work we did not explore added benefit from using CSF or Neurofilament-based biomarkers. Recent studies have shown high classification rates using such markers for differentiating Parkinson's Disease from atypical parkinsonisms (Angelopoulou, 2021; Quadalti, 2021; Schulz, 2021). In addition, some multi-modal studies have combined CSF or NfL markers with imaging and showed a marginal improvement over using only imaging data (Mangesius et al., 2020; Compta, 2022; Zhang, 2022).

Patient impact is expected to be greater when individual prediction is possible with a decision model, which requires validation in a large-scale clinical study. This will also facilitate recruitment for clinical trials for new drug development to improve treatment of parkinsonisms. This should be the direction of future work in this field.

Declaration of Competing Interest

The authors declare that they have no known competing financial interests or personal relationships that could have appeared to influence the work reported in this paper.

Data availability

The data that has been used is confidential.

Acknowledgements

We would like to thank Jan Gouman & Walter Deville, patient researchers from Parkinson Vereniging (Netherlands), for insightful discussions and their contribution towards shaping the methodology of this project. Dirk Poot (assistant professor, department of radiology, Erasmus MC) for insightful discussions towards the decision models, and for imaging software. We thank Elise Dopper (clinical researcher and neurologist, department of neurology, Erasmus MC) for helping in patient management and neurological scoring. We thank Tom Ruigrok (associate professor and neuroanatomist, department of neuroscience, Erasmus MC) for interpreting images from the brainstem.

References

Andersson, J.L.R., Skare, S., Ashburner, J., 2003. How to correct susceptibility distortions in spin-echo echo-planar images: application to diffusion tensor imaging. Neuroimage 20 (2), 870–888.

Andersson, J.L.R., Sotiropoulos, S.N., 2016. An integrated approach to correction for off-resonance effects and subject movement in diffusion MR imaging. Neuroimage 125, 1063–1078.

Angelopoulou, E., et al., 2021. CSF and Circulating NfL as Biomarkers for the Discrimination of Parkinson Disease From Atypical Parkinsonian Syndromes: Meta-analysis. Neurol Clin Pract 11 (6), e867–e875.

Archer, D.B., Bricker, J.T., Chu, W.T., Burciu, R.G., McCracken, J.L., Lai, S., Coombes, S. A., Fang, R., Barmpoutis, A., Corcos, D.M., Kurani, A.S., Mitchell, T., Black, M.L., Herschel, E., Simuni, T., Parrish, T.B., Comella, C., Xie, T., Seppi, K., Bohnen, N.I., Müller, M.L., Albin, R.L., Krismer, F., Du, G., Lewis, M.M., Huang, X., Li, H., Pasternak, O., McFarland, N.R., Okun, M.S., Vaillancourt, D.E., 2019. Development and validation of the automated imaging differentiation in parkinsonism (AID-P): a multicentre machine learning study. Lancet Digital Health 1 (5), e222–e231.

Bae, Y.J., Kim, J.-M., Kim, E., Lee, K.M., Kang, S.Y., Park, H.S., Kim, K.J., Kim, Y.E., Oh, E.S., Yun, J.Y., Kim, J.S., Jeong, H.-J., Jeon, B., Kim, S.E., 2016. Loss of Nigral hyperintensity on 3 Tesla MRI of Parkinsonism: comparison with (123) I-FP-CIT SPECT. Mov. Disord. 31 (5), 684–692.

Bae, Y.J., Kim, J.-M., Sohn, C.-H., Choi, J.-H., Choi, B.S., Song, Y.S., Nam, Y., Cho, S.J., Jeon, B., Kim, J.H., 2021. Imaging the substantia Nigra in Parkinson disease and other parkinsonian syndromes. Radiology 300 (2), 260–278.

Bluett, B., et al., 2021. Best practices in the clinical management of progressive supranuclear palsy and corticobasal syndrome: a consensus statement of the CurePSP centers of care. Front. Neurol. 12, 694872.

Bocchetta, M., Iglesias, J.E., Chelban, V., Jabbari, E., Lamb, R., Russell, L.L., Greaves, C. V., Neason, M., Cash, D.M., Thomas, D.L., Warren, J.D., Woodside, J., Houlden, H., Morris, H.R., Rohrer, J.D., 2020. Automated brainstem segmentation detects differential involvement in atypical Parkinsonian Syndromes. J. Mov. Disord. 13 (1), 39–46.

Chen, X., Huddleston, D.E., Langley, J., Ahn, S., Barnum, C.J., Factor, S.A., Levey, A.I., Hu, X., 2014. Simultaneous imaging of locus coeruleus and substantia nigra with a quantitative neuromelanin MRI approach. Magn. Reson. Imaging 32 (10), 1301–1306.

Chougar, L., et al., 2020. The role of magnetic resonance imaging for the diagnosis of atypical parkinsonism. Front. Neurol. 11, 665.

Chougar, L., et al., 2023. Comparison of mean diffusivity, R2* relaxation rate and morphometric biomarkers for the clinical differentiation of parkinsonism. Parkinsonism Relat. Disord. 108, 105287.

Chougar, L., Pyatigorskaya, N., Lehericy, S., 2021. Update on neuroimaging for categorization of Parkinson's disease and atypical parkinsonism. Curr. Opin. Neurol. 34 (4), 514–524.

Compta, Y., et al., 2022. Combined CSF alpha-SYN RT-QuIC, CSF NFL and midbrain-pons planimetry in degenerative parkinsonisms: From bedside to bench, and back again. Parkinsonism Relat. Disord. 99, 33–41.

Cozma, L., Avasilichioaei, M., Dima, N., Popescu, B.O., 2021. Of criteria and men-diagnosing atypical parkinsonism: towards an algorithmic approach. Brain Sci. 11 (6), 695.

Cui, X., Li, L., Yu, L., Xing, H., Chang, H., Zhao, L.i., Qian, J., Song, Q., Zhou, S., Dong, C., 2020. Gray matter atrophy in Parkinson's disease and the parkinsonian variant of multiple system atrophy: a combined ROI- and voxel-based morphometric study. Clinics 75, e1505.

Cure PSP – clinical trials.; Available from: https://www.psp.org/ineedsupport/clinical-trials/.

de Rochefort, L., Brown, R., Prince, M.R., Wang, Y.i., 2008. Quantitative MR susceptibility mapping using piece-wise constant regularized inversion of the magnetic field. Magn. Reson. Med. 60 (4), 1003–1009.

de Rochefort, L., Liu, T., Kressler, B., Liu, J., Spincemaille, P., Lebon, V., Wu, J., Wang, Y. i., 2010. Quantitative susceptibility map reconstruction from MR phase data using bayesian regularization: validation and application to brain imaging. Magn. Reson. Med. 63 (1), 194–206.

Deh, K., Nguyen, T.D., Eskreis-Winkler, S., Prince, M.R., Spincemaille, P., Gauthier, S., Kovanlikaya, I., Zhang, Y., Wang, Y.i., 2015. Reproducibility of quantitative susceptibility mapping in the brain at two field strengths from two vendors. J. Magn. Reson. Imaging 42 (6), 1592–1600.

Du, G., Lewis, M.M., Kanekar, S., Sterling, N.W., He, L., Kong, L., Li, R., Huang, X., 2017. Combined diffusion tensor imaging and apparent transverse relaxation rate differentiate parkinson disease and atypical parkinsonism. AJNR Am. J. Neuroradiol. 38 (5), 966–972.

Federatie Medisch Specialisten - Ziekte van Parkinson 2020.

Gaurav, R., et al., 2022. NigraNet: An automatic framework to assess nigral neuromelanin content in early Parkinson's disease using convolutional neural network. Neuroimage Clin 36, 103250.

He, N., et al., 2021. Imaging iron and neuromelanin simultaneously using a single 3D gradient echo magnetization transfer sequence: Combining neuromelanin, iron and the nigrosome-1 sign as complementary imaging biomarkers in early stage Parkinson's disease. Neuroimage 230, 117810.

Heim, B., Krismer, F., De Marzi, R., Seppi, K., 2017. Magnetic resonance imaging for the diagnosis of Parkinson's disease. J. Neural Transm. 124 (8), 915–964.

Heim, B., Krismer, F., Seppi, K., 2021. Differentiating PSP from MSA using MR planimetric measurements: a systematic review and meta-analysis. J. Neural Transm. (Vienna) 128 (10), 1497–1505.

Hughes, A.J., Daniel, S.E., Ben-Shlomo, Y., Lees, A.J., 2002. The accuracy of diagnosis of parkinsonian syndromes in a specialist movement disorder service. Brain 125 (4), 861–870.

Huppertz, H.-J., Möller, L., Südmeyer, M., Hilker, R., Hattingen, E., Egger, K., Amtage, F., Respondek, G., Stamelou, M., Schnitzler, A., Pinkhardt, E.H., Oertel, W.H., Knake, S., Kassubek, J., Höglinger, G.U., 2016. Differentiation of neurodegenerative parkinsonian syndromes by volumetric magnetic resonance imaging analysis and support vector machine classification. Mov. Disord. 31 (10), 1506–1517.

Iglesias, J.E., Van Leemput, K., Bhatt, P., Casillas, C., Dutt, S., Schuff, N., Truran-Sacrey, D., Boxer, A., Fischl, B., 2015. Bayesian segmentation of brainstem structures in MRI. Neuroimage 113, 184–195.

Isaias, I.U., et al., 2016. Neuromelanin imaging and dopaminergic loss in Parkinson's disease. Front. Aging Neurosci. 8, 196.

Jin, L., et al., 2019. Combined visualization of nigrosome-1 and neuromelanin in the substantia Nigra using 3T MRI for the differential diagnosis of essential tremor and de novo Parkinson's disease. Front. Neurol. 10, 100.

Joutsa, J., Gardberg, M., Röyttä, M., Kaasinen, V., 2014. Diagnostic accuracy of parkinsonism syndromes by general neurologists. Parkinsonism Relat. Disord. 20 (8), 840–844.

Kamagata, K., Zalesky, A., Hatano, T., Di Biase, M.A., El Samad, O., Saiki, S., Shimoji, K., Kumamaru, K.K., Kamiya, K., Hori, M., Hattori, N., Aoki, S., Pantelis, C., 2018. Connectome analysis with diffusion MRI in idiopathic Parkinson's disease: evaluation using multi-shell, multi-tissue, constrained spherical deconvolution. Neuroimage Clin. 17, 518–529.

Karsa, A., Punwani, S., Shmueli, K., 2019. The effect of low resolution and coverage on the accuracy of susceptibility mapping. Magn. Reson. Med. 81 (3), 1833–1848.

Kashihara, K., Shinya, T., Higaki, F., 2011. Reduction of neuromelanin-positive nigral volume in patients with MSA, PSP and CBD. Intern. Med. 50 (16), 1683–1687.

Kim, J., et al., 2022. Toward more accessible fully automated 3D volumetric MRI decision trees for the differential diagnosis of multiple system atrophy, related disorders, and age-matched healthy subjects. Cerebellum.

Kiryu, S., Yasaka, K., Akai, H., Nakata, Y., Sugomori, Y., Hara, S., Seo, M., Abe, O., Ohtomo, K., 2019. Deep learning to differentiate parkinsonian disorders separately using single midsagittal MR imaging: a proof of concept study. Eur. Radiol. 29 (12), 6891–6899.

Kressler, B., de Rochefort, L., Tian Liu, Spincemaille, P., Quan Jiang, Yi Wang, 2010. Nonlinear regularization for per voxel estimation of magnetic susceptibility distributions from MRI field maps. IEEE Trans. Med. Imaging 29 (2), 273–281.

Krismer, F., Seppi, K., Göbel, G., Steiger, R., Zucal, I., Boesch, S., Gizewski, E.R., Wenning, G.K., Poewe, W., Scherfler, C., 2019. Morphometric MRI profiles of multiple system atrophy variants and implications for differential diagnosis. Mov. Disord. 34 (7), 1041–1048.
Langkammer, C., Pirpamer, L., Seiler, S., Deistung, A., Schweser, F., Franthal, S., Homayoon, N., Katschnig-Winter, P., Koegl-Wallner, M., Pendl, T., Stoegerer, E.M., Wenzel, K., Fazekas, F., Ropele, S., Reichenbach, J.R., Schmidt, R., Schwingenschuh, P., Kassubek, J., 2016. Quantitative susceptibility mapping in Parkinson's disease. PLoS One 11 (9), e0162460.
Langley, J., Huddleston, D.E., Merritt, M., Chen, X., McMurray, R., Silver, M., Factor, S. A., Hu, X., 2016. Diffusion tensor imaging of the substantia nigra in Parkinson's disease revisited. Hum. Brain Mapp. 37 (7), 2547–2556.
Lehericy, S., Vaillancourt, D.E., Seppi, K., Monchi, O., Rektorova, I., Antonini, A., McKeown, M.J., Masellis, M., Berg, D., Rowe, J.B., Lewis, S.J.G., Williams-Gray, C. H., Tessitore, A., Siebner, H.R., 2017. The role of high-field magnetic resonance imaging in parkinsonian disorders: pushing the boundaries forward. Mov. Disord. 32 (4), 510–525.
Leng, Y., et al., *Stratified Parkinsonism classification based on multi-modality MRI. Proc. Intl. Soc. Mag. Reson. Med. 30. 2951*. 2022.
Liu, T., Khalidov, I., de Rochefort, L., Spincemaille, P., Liu, J., Tsiouris, A.J., Wang, Y.i., 2011. A novel background field removal method for MRI using projection onto dipole fields (PDF). NMR Biomed. 24 (9), 1129–1136.
Liu, T., Wisnieff, C., Lou, M., Chen, W., Spincemaille, P., Wang, Y.i., 2013. Nonlinear formulation of the magnetic field to source relationship for robust quantitative susceptibility mapping. Magn. Reson. Med. 69 (2), 467–476.
Ma, K.K.Y., Lin, S., Mok, V.C.T., 2019. Neuroimaging in vascular parkinsonism. Curr. Neurol. Neurosci. Rep. 19 (12), 102.
Mangesius, S., Hussl, A., Krismer, F., Mahlknecht, P., Reiter, E., Tagwercher, S., Djamshidian, A., Schocke, M., Esterhammer, R., Wenning, G., Müller, C., Scherfler, C., Gizewski, E.R., Poewe, W., Seppi, K., 2018. MR planimetry in neurodegenerative parkinsonism yields high diagnostic accuracy for PSP. Parkinson. Relat. Disord. 46, 47–55.
Mangesius, S., Mariotto, S., Ferrari, S., Pereverzyev, S., Lerchner, H., Haider, L., Gizewski, E.R., Wenning, G., Seppi, K., Reindl, M., Poewe, W., 2020. Novel decision algorithm to discriminate parkinsonism with combined blood and imaging biomarkers. Parkinsonism Relat. Disord. 77, 57–63.
Marsili, L., Rizzo, G., Colosimo, C., 2018. Diagnostic criteria for Parkinson's disease: from James Parkinson to the concept of prodromal disease. Front. Neurol. 9, 156.
Massey, L.A., Jager, H.R., Paviour, D.C., O'Sullivan, S.S., Ling, H., Williams, D.R., Kallis, C., Holton, J., Revesz, T., Burn, D.J., Yousry, T., Lees, A.J., Fox, N.C., Micallef, C., 2013. The midbrain to pons ratio: a simple and specific MRI sign of progressive supranuclear palsy. Neurology 80 (20), 1856–1861.
Mazzucchi, S., et al., 2019. Quantitative susceptibility mapping in atypical Parkinsonisms. Neuroimage Clin. 24, 101999.
Meijer, F.J.A., van Rumund, A., Fasen, B.A.C.M., Titulaer, I., Aerts, M., Esselink, R., Bloem, B.R., Verbeek, M.M., Goraj, B., 2015. Susceptibility-weighted imaging improves the diagnostic accuracy of 3T brain MRI in the work-up of parkinsonism. AJNR Am. J. Neuroradiol. 36 (3), 454–460.
Meijer, F.J.A., Steens, S.C., van Rumund, A., van Cappellen van Walsum, A.-M., Küsters, B., Esselink, R.A.J., Verbeek, M.M., Bloem, B.R., Goraj, B., 2016. Nigrosome-1 on susceptibility weighted imaging to differentiate Parkinson's disease from atypical Parkinsonism: an in vivo and ex vivo pilot study. Pol. J. Radiol. 81, 363–369.
Messina, D., Cerasa, A., Condino, F., Arabia, G., Novellino, F., Nicoletti, G., Salsone, M., Morelli, M., Lanza, P.L., Quattrone, A., 2011. Patterns of brain atrophy in Parkinson's disease, progressive supranuclear palsy and multiple system atrophy. Parkinsonism Relat. Disord. 17 (3), 172–176.
Min, J., Park, M., Choi, J.W., Jahng, G.-H., Moon, W.-J., 2018. Inter-vendor and inter-session reliability of diffusion tensor imaging: implications for multicenter clinical imaging studies. Korean J. Radiol. 19 (4), 777.
Mitchell, T., Archer, D.B., Chu, W.T., Coombes, S.A., Lai, S., Wilkes, B.J., McFarland, N. R., Okun, M.S., Black, M.L., Herschel, E., Simuni, T., Comella, C., Xie, T., Li, H., Parrish, T.B., Kurani, A.S., Corcos, D.M., Vaillancourt, D.E., 2019. Neurite orientation dispersion and density imaging (NODDI) and free-water imaging in Parkinsonism. Hum. Brain Mapp. 40 (17), 5094–5107.
Möller, L., et al., 2017. Manual MRI morphometry in Parkinsonian syndromes. Mov. Disord. 32 (5), 778–782.
National Institute for Health and Care Excellence - Parkinson's disease in Adults. 2017.
Nicoletti, G., Fera, F., Condino, F., Auteri, W., Gallo, O., Pugliese, P., Arabia, G., Morgante, L., Barone, P., Zappia, M., Quattrone, A., 2006. MR imaging of middle cerebellar peduncle width: differentiation of multiple system atrophy from Parkinson disease. Radiology 239 (3), 825–830.
Oba, H., Yagishita, A., Terada, H., Barkovich, A.J., Kutomi, K., Yamauchi, T., Furui, S., Shimizu, T., Uchigata, M., Matsumura, K., Sonoo, M., Sakai, M., Takada, K., Harasawa, A., Takeshita, K., Kohtake, H., Tanaka, H., Suzuki, S., 2005. New and reliable MRI diagnosis for progressive supranuclear palsy. Neurology 64 (12), 2050–2055.
Ogisu, K., Kudo, K., Sasaki, M., Sakushima, K., Yabe, I., Sasaki, H., Terae, S., Nakanishi, M., Shirato, H., 2013. 3D neuromelanin-sensitive magnetic resonance imaging with semi-automated volume measurement of the substantia nigra pars compacta for diagnosis of Parkinson's disease. Neuroradiology 55 (6), 719–724.
Ohtsuka, C., Sasaki, M., Konno, K., Kato, K., Takahashi, J., Yamashita, F., Terayama, Y., 2014. Differentiation of early-stage parkinsonisms using neuromelanin-sensitive magnetic resonance imaging. Parkinsonism Relat. Disord. 20 (7), 755–760.
Oshima, S., et al., 2021. Neuromelanin-sensitive magnetic resonance imaging using DANTE pulse. Mov. Disord. 36 (4), 874–882.
Pasternak, O., Sochen, N., Gur, Y., Intrator, N., Assaf, Y., 2009. Free water elimination and mapping from diffusion MRI. Magn. Reson. Med. 62 (3), 717–730.
Pavese, N., Tai, Y.F., 2018. Nigrosome imaging and neuromelanin sensitive MRI in diagnostic evaluation of parkinsonism. Mov. Disord. Clin. Pract. 5 (2), 131–140.
Peralta, C., Strafella, A.P., van Eimeren, T., Ceravolo, R., Seppi, K., Kaasinen, V., Arena, J.E., Lehericy, S., 2022. Pragmatic approach on neuroimaging techniques for the differential diagnosis of Parkinsonisms. Mov. Disord. Clin. Pract. 9 (1), 6–19.
Planetta, P.J., Ofori, E., Pasternak, O., Burciu, R.G., Shukla, P., DeSimone, J.C., Okun, M. S., McFarland, N.R., Vaillancourt, D.E., 2016. Free-water imaging in Parkinson's disease and atypical parkinsonism. Brain 139 (2), 495–508.
Poewe, W., Seppi, K., Tanner, C.M., Halliday, G.M., Brundin, P., Volkmann, J., Schrag, A.-E., Lang, A.E., 2017. Parkinson disease. Nat. Rev. Dis. Primers 3 (1).
Poewe, W., Stankovic, I., Halliday, G., Meissner, W.G., Wenning, G.K., Pellecchia, M.T., Seppi, K., Palma, J.-A., Kaufmann, H., 2022. Multiple system atrophy. Nat. Rev. Dis. Primers 8 (1).
Priovoulos, N., Jacobs, H.I.L., Ivanov, D., Uludağ, K., Verhey, F.R.J., Poser, B.A., 2018. High-resolution in vivo imaging of human locus coeruleus by magnetization transfer MRI at 3T and 7T. Neuroimage 168, 427–436.
Pyatigorskaya, N., et al., 2020. Iron imaging as a diagnostic tool for Parkinson's disease: a systematic review and meta-analysis. Front. Neurol. 11, 366.
Pyatigorskaya, N., Yahia-Cherif, L., Gaurav, R., Ewenczyk, C., Gallea, C., Valabregue, R., Gargouri, F., Magnin, B., Degos, B., Roze, E., Bardinet, E., Poupon, C., Arnulf, I., Vidailhet, M., Lehericy, S., 2020. Multimodal magnetic resonance imaging quantification of brain changes in progressive supranuclear palsy. Mov. Disord. 35 (1), 161–170.
Quadalti, C., et al., 2021. Neurofilament light chain and alpha-synuclein RT-QuIC as differential diagnostic biomarkers in parkinsonisms and related syndromes. NPJ Parkinsons. Dis. 7 (1), 93.
Quattrone, A., Nicoletti, G., Messina, D., Fera, F., Condino, F., Pugliese, P., Lanza, P., Barone, P., Morgante, L., Zappia, M., Aguglia, U., Gallo, O., 2008. MR imaging index for differentiation of progressive supranuclear palsy from Parkinson disease and the Parkinson variant of multiple system atrophy. Radiology 246 (1), 214–221.
Quattrone, A., Morelli, M., Nigro, S., Quattrone, A., Vescio, B., Arabia, G., Nicoletti, G., Nisticò, R., Salsone, M., Novellino, F., Barbagallo, G., Le Piane, E., Pugliese, P., Bosco, D., Vaccaro, M.G., Chiriaco, C., Sabatini, U., Vescio, V., Stanà, C., Rocca, F., Gullà, D., Caracciolo, M., 2018. A new MR imaging index for differentiation of progressive supranuclear palsy-parkinsonism from Parkinson's disease. Parkinsonism Relat. Disord. 54, 3–8.
Salvatore, C., Cerasa, A., Castiglioni, I., Gallivanone, F., Augimeri, A., Lopez, M., Arabia, G., Morelli, M., Gilardi, M.C., Quattrone, A., 2014. Machine learning on brain MRI data for differential diagnosis of Parkinson's disease and Progressive Supranuclear Palsy. J. Neurosci. Methods 222, 230–237.
Santin, M.D., et al., 2017. Reproducibility of R2 * and quantitative susceptibility mapping (QSM) reconstruction methods in the basal ganglia of healthy subjects. NMR Biomed. 30 (4).
Sasaki, M., Shibata, E., Tohyama, K., Takahashi, J., Otsuka, K., Tsuchiya, K., Takahashi, S., Ehara, S., Terayama, Y., Sakai, A., 2006. Neuromelanin magnetic resonance imaging of locus ceruleus and substantia nigra in Parkinson's disease. Neuroreport 17 (11), 1215–1218.
Scherfler, C., Göbel, G., Müller, C., Nocker, M., Wenning, G.K., Schocke, M., Poewe, W., Seppi, K., 2016. Diagnostic potential of automated subcortical volume segmentation in atypical parkinsonism. Neurology 86 (13), 1242–1249.
Schulz, I., et al., 2021. Systematic assessment of 10 biomarker candidates focusing on alpha-synuclein-related disorders. Mov. Disord. 36 (12), 2874–2887.
Schwarz, S.T., Abaei, M., Gontu, V., Morgan, P.S., Bajaj, N., Auer, D.P., 2013. Diffusion tensor imaging of nigral degeneration in Parkinson's disease: a region-of-interest and voxel-based study at 3T and systematic review with meta-analysis. Neuroimage Clin 3, 481–488.
Shao, N., et al., 2014. Voxelwise meta-analysis of gray matter anomalies in progressive supranuclear palsy and Parkinson's disease using anatomic likelihood estimation. Front. Hum. Neurosci. 8, 63.
Shao, N., Yang, J., Shang, H., 2015. Voxelwise meta-analysis of gray matter anomalies in Parkinson variant of multiple system atrophy and Parkinson's disease using anatomic likelihood estimation. Neurosci. Lett. 587, 79–86.
Simões, R.M., Castro Caldas, A., Grilo, J., Correia, D., Guerreiro, C., Pita Lobo, P., Valadas, A., Fabbri, M., Correia Guedes, L., Coelho, M., Rosa, M.M., Ferreira, J.J., Reimão, S., 2020. A distinct neuromelanin magnetic resonance imaging pattern in parkinsonian multiple system atrophy. BMC Neurol. 20 (1).
Sjöström, H., Granberg, T., Westman, E., Svenningsson, P., 2017. Quantitative susceptibility mapping differentiates between parkinsonian disorders. Parkinsonism Relat. Disord. 44, 51–57.
Stamelou, M., Respondek, G., Giagkou, N., Whitwell, J.L., Kovacs, G.G., Höglinger, G.U., 2021. Evolving concepts in progressive supranuclear palsy and other 4-repeat tauopathies. Nat. Rev. Neurol. 17 (10), 601–620.
Stoessl, A.J., Lehericy, S., Strafella, A.P., 2014. Imaging insights into basal ganglia function, Parkinson's disease, and dystonia. Lancet 384 (9942), 532–544.
Sulzer, D., et al., 2018. Neuromelanin detection by magnetic resonance imaging (MRI) and its promise as a biomarker for Parkinson's disease. NPJ Parkinsons Dis. 4, 11.
Takahashi, H., et al., 2018. Quantifying changes in nigrosomes using quantitative susceptibility mapping and neuromelanin imaging for the diagnosis of early-stage Parkinson's disease. Br. J. Radiol. 91 (1086), 20180037.
Talai, A.S., et al., 2021. Utility of multi-modal MRI for differentiating of Parkinson's disease and progressive supranuclear palsy using machine learning. Front. Neurol. 12, 648548.
Topgaard, D., 2017. Multidimensional diffusion MRI. J. Magn. Reson. 275, 98–113.

Trujillo, P., Summers, P.E., Ferrari, E., Zucca, F.A., Sturini, M., Mainardi, L.T., Cerutti, S., Smith, A.K., Smith, S.A., Zecca, L., Costa, A., 2017. Contrast mechanisms associated with neuromelanin-MRI. Magn. Reson. Med. 78 (5), 1790–1800.

van der Pluijm, M., Cassidy, C., Zandstra, M., Wallert, E., de Bruin, K., Booij, J., de Haan, L., Horga, G., van de Giessen, E., 2021. Reliability and reproducibility of neuromelanin-sensitive imaging of the Substantia Nigra: a comparison of three different sequences. J. Magn. Reson. Imaging 53 (3), 712–721.

Wang, Y.i., Spincemaille, P., Liu, Z., Dimov, A., Deh, K., Li, J., Zhang, Y., Yao, Y., Gillen, K.M., Wilman, A.H., Gupta, A., Tsiouris, A.J., Kovanlikaya, I., Chiang, G.-Y., Weinsaft, J.W., Tanenbaum, L., Chen, W., Zhu, W., Chang, S., Lou, M., Kopell, B.H., Kaplitt, M.G., Devos, D., Hirai, T., Huang, X., Korogi, Y., Shtilbans, A., Jahng, G.-H., Pelletier, D., Gauthier, S.A., Pitt, D., Bush, A.I., Brittenham, G.M., Prince, M.R., 2017. Clinical quantitative susceptibility mapping (QSM): Biometal imaging and its emerging roles in patient care. J. Magn. Reson. Imaging 46 (4), 951–971.

Wengler, K., et al., 2021. Cross-scanner harmonization of neuromelanin-sensitive MRI for multisite studies. J. Magn. Reson. Imaging 54 (4), 1189–1199.

Wenning, G.K., Stankovic, I., Vignatelli, L., Fanciulli, A., Calandra-Buonaura, G., Seppi, K., Palma, J.-A., Meissner, W.G., Krismer, F., Berg, D., Cortelli, P., Freeman, R., Halliday, G., Höglinger, G., Lang, A., Ling, H., Litvan, I., Low, P., Miki, Y., Panicker, J., Pellecchia, M.T., Quinn, N., Sakakibara, R., Stamelou, M., Tolosa, E., Tsuji, S., Warner, T., Poewe, W., Kaufmann, H., 2022. The movement disorder society criteria for the diagnosis of multiple system atrophy. Mov. Disord. 37 (6), 1131–1148.

Worker, A., Blain, C., Jarosz, J., Chaudhuri, K.R., Barker, G.J., Williams, S.C.R., Brown, R.G., Leigh, P.N., Dell'Acqua, F., Simmons, A., Kassubek, J., 2014. Diffusion tensor imaging of Parkinson's disease, multiple system atrophy and progressive supranuclear palsy: a tract-based spatial statistics study. PLoS One 9 (11), e112638.

Zhang, P., et al., 2022. Quantitative susceptibility mapping and blood neurofilament light chain differentiate between parkinsonian disorders. Front. Aging Neurosci. 14, 909552.

Zhang, Y., Burock, M.A., 2020. Diffusion tensor imaging in parkinson's disease and parkinsonian syndrome: a systematic review. Front. Neurol. 11, 531993.